High-energy photons in neutron-proton and proton-nucleus collisions

K. Nakayama

Department of Physics and Astronomy, University of Georgia, Athens, Georgia 30602

(Received 11 July 1988)

In an effort to better understand the dynamics of nucleon-nucleon bremsstrahlung in producing energetic photons, we have investigated the contribution of each part of the current associated with the different terms in the nuclear Hamiltonian to the neutron-proton bremsstrahlung cross sections. In the range of photon energy investigated here, we find meson-exchange currents to be the dominant source of high-energy photons ($\omega \gtrsim 50$ MeV). Although the one-body current contribution is small for such energetic photons, its interference with the two-body current is important and enhances the cross section. At low photon energy the convection current dominates. We find that the bremsstrahlung cross section is very sensitive to the $^3(SD)_1$ states and offers a potential means of investigating short-range correlation effects. Off-energy-shell effects are estimated to have only a small influence on the neutron-proton bremsstrahlung inclusive cross section. In connection with the neutron-proton bremsstrahlung process, the nucleon-nucleon collisional mechanism in producing high-energy photons in proton-induced reactions has been also investigated within the nuclear matter approximation. Nuclear medium effects in *intermediate* states are shown to have a minor influence on the photon cross section; therefore, the use of a free nucleon-nucleon T matrix instead of a G matrix seems to be well justified. However, the results are found to be very sensitive to medium effects in the initial and final states.

I. INTRODUCTION

Because of the weak electromagnetic coupling, photonuclear reactions constitute an interesting area for both theoretical and experimental testing of nuclear reaction dynamics. For example, both radiative capture and photodisintegration reactions are of interest as mechanisms which, at medium to high energies, provide a method for investigating processes involving a large momentum transfer to a nucleus.[1,2] Very recently, the observation of energetic photons produced in heavy ion collisions[3-6] has stimulated a considerable effort toward explaining the production mechanism of these high-energy photons.[7-14] Among the different mechanisms suggested, theoretical calculations seem to indicate the incoherent neutron-proton (np) collisional bremsstrahlung to be the most likely source of these energetic photons. However, with the exception of Ref. 13, all reported calculations are based on the simple bremsstrahlung formula (and its offspring) derived by taking into account only the convection current contribution. The importance of meson-exchange currents in photon production (radiative capture reactions and np bremsstrahlung) has been reported by several authors.[1,15] In particular, in order to account for the existing experimental np bremsstrahlung data, the inclusion of the meson-exchange process which increases the photon cross section by a factor ~ 2 appears essential.[15] Therefore, before any definitive conclusion can be drawn about the role of the nucleon-nucleon (NN) collisional process on energetic photon production in heavy ion collisions, one has to understand thoroughly the dynamics of the elementary process. Although a free T matrix was used in the calculations by Neuhauser and Koonin,[13] they included not only the convection current,

but also meson-exchange and magnetization current contributions.

In the present paper, we analyze in some detail (in Secs. II and III) the role of each part of the current associated wit the different terms in the nuclear Hamiltonian on the elementary np bremsstrahlung cross section in an attempt to better understand the dynamics. In Secs. IV and V we investigate the influence of the nuclear medium by studying proton-nucleus bremsstrahlung within the nuclear matter approximation. In Sec. VI some conclusions are given.

II. NUCLEON-NUCLEON BREMSSTRAHLUNG

The photon production amplitude in a NN collision is evaluated within the nonrelativistic formulation, where the strong interaction is treated to all orders in perturbation theory and the coupling to the photon is taken only to first order. There are several previous calculations of NN photon production cross sections within such a scheme.[15-17] We follow closely the formalism of Ref. 15 in which the gauge invariance of the complete nucleon-nucleon-photon (NNγ) amplitude is required. The only difference is that here we express all the quantities in momentum space rather than in coordinate space. For the sake of completeness, and the definition of the terms referred to later, we give below a few steps of the derivation of the photon emission amplitude and exhibit its explicit form. For the details we refer to Ref. 15.

The transition amplitude M for producing a photon of momentum k and polarization ϵ in a NN collision is written as

$$M = \langle \epsilon, \mathbf{k}; \psi_f^- | V_{\text{em}} | 0; \psi_i^+ \rangle \ , \tag{2.1}$$

where V_{em} stands for the photon emission potential and ψ_i^+ (ψ_f^-) denotes the wave function of strongly interacting two nucleons in the initial (final) state. The superscript $+$ or $-$ indicates the boundary condition associated with the outgoing ($+$) or incoming ($-$) waves. The wave function ψ can be expressed in terms of the T matrix as

$$|\psi^\pm\rangle = |\phi\rangle + \frac{1}{E^\pm} T^\pm |\phi\rangle \ . \tag{2.2}$$

Here, ϕ denotes the unperturbed wave function, $E^\pm$ is the energy denominator, and $T^\pm$ stands for the T matrix.

Substituting Eq. (2.2) into Eq. (2.1) one obtains

$$M = \langle \epsilon, \mathbf{k}; \phi_f | V_{\text{em}} | 0; \phi_i \rangle + \left\langle \epsilon, \mathbf{k}; \phi_f \left| (T^-)^\dagger \frac{1}{E_f} V_{\text{em}} \right| 0; \phi_i \right\rangle$$

$$+ \left\langle \epsilon, \mathbf{k}; \phi_f \left| V_{\text{em}} \frac{1}{E_i} T^+ \right| 0; \phi_i \right\rangle$$

$$+ \left\langle \epsilon, \mathbf{k}; \phi_f \left| (T^-)^\dagger \frac{1}{E_f} V_{\text{em}} \frac{1}{E_i} T^+ \right| 0; \phi_i \right\rangle \ , \tag{2.3}$$

where the superscripts $+$ in the energy denominators have been omitted, since in the above equation they have the same boundary conditions, i.e., $E_{i,f} = E_{i,f}^+$. The first term in Eq. (2.3) is referred to as zero-scattering, the second and third terms as single-scattering, and the last one as the double- or rescattering contributions.

The transition operator (photon emission potential) V_{em} consists of three terms:

$$V_{\text{em}} = V_{\text{conv}} + V_{\text{magn}} + V_{\text{exch}} \ , \tag{2.4}$$

where V_{conv} denotes the contribution from the convection current, V_{magn} is from the magnetization current, and the last term V_{exch} denotes the contribution from the NN interaction due to its momentum dependence and includes the meson-exchange as well as the nonlocal currents. V_{conv} and V_{magn} constitute the one-body current, while V_{exch} is the two-body current. The single-scattering contributions due to the one-body current are also referred to as the external radiation, while the remaining terms are referred to as the internal radiation.

In momentum space, V_{conv} and V_{magn} take the forms (in the NN center-of-mass frame)

$$V_{\text{conv}}(\mathbf{p}', \mathbf{p}) = -\sqrt{2\pi/k} \, \frac{\boldsymbol{\epsilon} \cdot (\mathbf{p}' + \mathbf{p})}{2m} [e_1 \delta(\mathbf{p} - \mathbf{p}' - \mathbf{k}/2)$$

$$- e_2 \delta(\mathbf{p} - \mathbf{p}' + \mathbf{k}/2)] \ , \tag{2.5a}$$

$$V_{\text{magn}}(\mathbf{p}', \mathbf{p}) = i\sqrt{2\pi/k} \, \frac{e}{2m}$$

$$\times [\mu_1 \boldsymbol{\sigma}_1 \cdot (\mathbf{k} \wedge \boldsymbol{\epsilon}) \delta(\mathbf{p} - \mathbf{p}' - \mathbf{k}/2)$$

$$+ \mu_2 \boldsymbol{\sigma}_2 \cdot (\mathbf{k} \wedge \boldsymbol{\epsilon}) \delta(\mathbf{p} - \mathbf{p}' + \mathbf{k}/2)] \ , \tag{2.5b}$$

where $\mathbf{p}$ and $\mathbf{p}'$ denote the momenta of the interacting nucleons before and after the action of the photon emission potential; m stands for the mass of the nucleon; e_1 and e_2

are the electric charges of the interacting nucleons 1 and 2 (e for protons and 0 for neutrons); μ_1 and μ_2 are the magnetic moments of the interacting nucleons in units of nuclear magneton (2.793 for protons and -1.913 for neutrons); and $\boldsymbol{\sigma}_1$ and $\boldsymbol{\sigma}_2$ are the Pauli spin matrices.

The induced electromagnetic potential V_{exch} is obtained in the soft-photon limit[15] which in momentum space is given by

$$V_{\text{exch}}(\mathbf{p}', \mathbf{p}) = \sqrt{2\pi/k} \, \frac{\boldsymbol{\epsilon}}{2} \cdot \{ (e_2' - e_1')[\nabla_{\mathbf{p}'} V(\mathbf{p}', \mathbf{p})]$$

$$+ (e_2 - e_1)[\nabla_{\mathbf{p}} V(\mathbf{p}', \mathbf{p})] \} \ , \tag{2.6}$$

where $V(\mathbf{p}', \mathbf{p})$ denotes the bare NN potential. As one sees explicitly, the two-body current in the soft-photon limit contributes only to the np bremsstrahlung reaction. Within the meson-exchange model of the nuclear force, the one-pion-exchange contribution should be the dominant one in Eq. (2.6), since the pion has the lightest mass among the exchanged mesons and consequently the potential associated with it has the strongest momentum dependence.

The validity of the soft-photon approximation for V_{exch} has been discussed in Refs. 15 and 18, where it is shown that it is a good approximation even for considerably high-energy photons.[18] As we shall show later, our estimate also supports this.

The convection and the magnetization current parts of V_{em} in Eq. (2.4) do not contribute to the first term in Eq. (2.3) because of energy and momentum conservation. In Ref. 19 it is shown that, in the soft-photon limit, a part of the rescattering term from the one-body current cancels precisely the contribution from the two-body current, so that the current conservation is assured in that limit. However, Brown and Franklin[15] have found that the influence of the rescattering term from the one-body current to the cross section is rather small. Although the kinematical situation studied in Ref. 15 is very different from those in which we are interested here, and therefore the rescattering contribution from the one-body current might not necessarily be small in the present case, we have omitted this contribution entirely. (Work to include this rescattering term from the one-body current is currently in progress.) The rescattering contribution from V_{exch} has been included.

Because the T-matrix elements are usually calculated in the NN center-of-mass (c.m.) frame, it is convenient to evaluate each term in the right-hand side of Eq. (2.3) in an appropriate frame. For example, the third term is calculated in the initial NN c.m. frame, while the second one may be evaluated in the final NN c.m. frame which is shifted by $-\mathbf{k}$ with respect to the initial NN c.m. frame. The transformation from one system to the other (and also to the laboratory frame) is made relativistically, consistent with the relativistic treatment of the two-nucleon kinematics. This is particularly important if one tries to describe angular distributions.

Then, each contribution in Eq. (2.3) takes a simple form in momentum space. For the convection current one has

$$\left\langle \epsilon, \mathbf{k}; \phi_{\mathbf{p}'}^{S'M'_S} \middle| (T^-)^\dagger \frac{1}{E_f} V_{\text{conv}} \middle| 0; \phi_{\mathbf{p}}^{SM_S} \right\rangle$$

$$= -\sqrt{2\pi/k}\, \delta_{SS'} \frac{\epsilon \cdot \mathbf{p}}{m} \left[e_1 \frac{\langle \mathbf{p}', SM'_S | (T^-)^\dagger | \mathbf{p} - \mathbf{k}/2, SM_S \rangle}{E(|\mathbf{p} - \mathbf{k}/2|, p')} - e_2 \frac{\langle \mathbf{p}', SM'_S | (T^-)^\dagger | \mathbf{p} + \mathbf{k}/2, SM_S \rangle}{E(|\mathbf{p} + \mathbf{k}/2|, p')} \right], \quad (2.7a)$$

and

$$\left\langle \epsilon, \mathbf{k}; \phi_{\mathbf{p}'}^{S'M'_S} \middle| V_{\text{conv}} \frac{1}{E_i} T^+ \middle| 0; \phi_{\mathbf{p}}^{SM_S} \right\rangle$$

$$= -\sqrt{2\pi/k}\, \delta_{SS'} \frac{\epsilon \cdot \mathbf{p}'}{m} \left[e_1 \frac{\langle \mathbf{p}' + \mathbf{k}/2, SM'_S | T^+ | \mathbf{p}, SM_S \rangle}{E(|\mathbf{p}' + \mathbf{k}/2|, p)} - e_2 \frac{\langle \mathbf{p}' - \mathbf{k}/2, SM'_S | T^+ | \mathbf{p}, SM_S \rangle}{E(|\mathbf{p}' - \mathbf{k}/2|, p)} \right], \quad (2.7b)$$

where we have explicitly

$$E(p', p) = 2[\varepsilon(p') - \varepsilon(p)] + i\eta \tag{2.8a}$$

with

$$\varepsilon(p) \equiv (p^2 + m^2)^{1/2}. \tag{2.8b}$$

S (S') and M_S (M'_S) denote total spin and its projection in the initial (final) state. Analogously, for the magnetization current

$$\left\langle \epsilon, \mathbf{k}; \phi_{\mathbf{p}'}^{S'M'_S} \middle| (T^-)^\dagger \frac{1}{E_f} V_{\text{magn}} \middle| 0; \phi_{\mathbf{p}}^{SM_S} \right\rangle$$

$$= i\sqrt{2\pi/k}\, \frac{e}{2m} \sum_{M''_S} \left[\mu_1 \frac{\langle \mathbf{p}', S'M'_S | (T^-)^\dagger | \mathbf{p} - \mathbf{k}/2, S'M''_S \rangle \langle S'M''_S | \sigma_1 \cdot (\mathbf{k} \wedge \epsilon) | SM_S \rangle}{E(|\mathbf{p} - \mathbf{k}/2|, p')} \right.$$

$$\left. + \mu_2 \frac{\langle \mathbf{p}', S'M'_S | (T^-)^\dagger | \mathbf{p} + \mathbf{k}/2, S'M''_S \rangle \langle S'M''_S | \sigma_2 \cdot (\mathbf{k} \wedge \epsilon) | SM_S \rangle}{E(|\mathbf{p} + \mathbf{k}/2|, p')} \right], \quad (2.9a)$$

and

$$\left\langle \epsilon, \mathbf{k}; \phi_{\mathbf{p}'}^{S'M'_S} \middle| V_{\text{magn}} \frac{1}{E_i} T^+ \middle| 0; \phi_{\mathbf{p}}^{SM_S} \right\rangle = i\sqrt{2\pi/k}\, \frac{e}{2m} \sum_{M''_S} \left[\mu_1 \frac{\langle S'M'_S | \sigma_1 \cdot (\mathbf{k} \wedge \epsilon) | SM''_S \rangle \langle \mathbf{p}' + \mathbf{k}/2, SM''_S | T^+ | \mathbf{p}, SM_S \rangle}{E(|\mathbf{p}' + \mathbf{k}/2|, p)} \right.$$

$$\left. + \mu_2 \frac{\langle S'M'_S | \sigma_2 \cdot (\mathbf{k} \wedge \epsilon) | SM''_S \rangle \langle \mathbf{p}' - \mathbf{k}/2, SM''_S | T^+ | \mathbf{p}, SM_S \rangle}{E(|\mathbf{p}' - \mathbf{k}/2|, p)} \right].$$

$$(2.9b)$$

We notice that Eqs. (2.7a) and (2.9a) are expressed in the final NN c.m. frame, with Eqs. (2.7b) and (2.9b) in the initial NN c.m. frame.

The T-matrix elements in Eqs. (2.7) and (2.9) are expressed in the standard partial wave decomposition

$$\langle \mathbf{p}', SM'_S | T^\pm | \mathbf{p}, SM_S \rangle = \frac{2}{\pi} \sum_{LL'J} \sum_{M_L M'_L M_J} i^{L-L'} (SM_S L M_L | J M_J)(SM'_S L'M'_L | J M_J) Y_{L'M'_L}(\hat{\mathbf{p}}') Y^*_{LM_L}(\hat{\mathbf{p}}) T^{JST\pm}_{L'L}(p', p) P_T,$$

$$(2.10)$$

where J, L (L'), and T denote the total angular momentum, the orbital angular momentum, and the total isospin, respectively. M_J, and M_L (M'_L) are the projections of total and orbital spin angular momentum. P_T denotes the isospin projection operator. Here the partial wave T-matrix elements obey the relation

$$T^{JST+}_{L'L}(p', p) = [T^{JST-}_{L'L}(p', p)]^*. \tag{2.11}$$

Since the two-nucleon state can be expressed as a linear combination of states with definite total isospin T, the evaluation of the NN T-matrix elements in Eqs. (2.7) and (2.9) involves a summation over the isospin quantum number T and a proper normalization factor. For example, for the np bremsstrahlung

$$|np\rangle = \frac{1}{\sqrt{2}}(|T=1, M_T=0\rangle + |T=0, M_T=0\rangle), \tag{2.12}$$

so that the np T-matrix elements are obtained by summing over the isospin T and multiplying by an overall factor $\frac{1}{2}$.

The spin matrix elements in Eq. (2.9) can be easily expressed as

$$\langle S'M_S'|\sigma_1\cdot\mathbf{a}|SM_S\rangle = \sqrt{6}(-)^S[S]\begin{bmatrix}\frac{1}{2} & S' & \frac{1}{2} \\ S & \frac{1}{2} & 1\end{bmatrix}$$

$$\times\sum_m(-)^m(SM_S1m|S'M_S')a_{-m} ,$$

(2.13a)

$$\langle S'M_S'|\sigma_2\cdot\mathbf{a}|SM_S\rangle = (-)^{S'-S}\langle S'M_S'|\sigma_1\cdot\mathbf{a}|SM_S\rangle ,$$

(2.13b)

where $[S]\equiv\sqrt{2S+1}$.

The two-body current contribution to the photon emission amplitude is most easily calculated starting directly from Eq. (2.1) and noticing that (omitting the superscript $+$ or $-$ for simplicity of notation)

$$T(\mathbf{p}',\mathbf{p}) = \int d^3p'' V(\mathbf{p}',\mathbf{p}'')\psi_\mathbf{p}(\mathbf{p}'') .$$

(2.14)

We obtain

$$\langle\epsilon,\mathbf{k};\psi_{\mathbf{p}'}^-|V_{\text{exch}}|0;\psi_\mathbf{p}^+\rangle = \int d^3p'' \left[\psi_{\mathbf{p}'}^{-*}(\mathbf{p}'')\left[\frac{(\tau_1'-\tau_2')_z}{2}\right][\nabla_{\mathbf{p}''}T^+(\mathbf{p}'',\mathbf{p})] + [\nabla_{\mathbf{p}'}(T^-(\mathbf{p}'',\mathbf{p}))^\dagger]\left[\frac{(\tau_1-\tau_2)_z}{2}\right]\psi_\mathbf{p}^+(\mathbf{p}'')\right] ,$$

(2.15a)

where $(\tau_i)_z$ denotes the z component of the isospin operator τ_i of the nucleon i, so that

$$e_i = \frac{1}{2}[1-(\tau_i)_z] ,$$

(2.15b)

in the nuclear physics convention.

Using the partial wave decomposition of the T matrix [see Eq. (2.10)] and the wave function

$$\psi_\mathbf{p}^{SM_S}(\mathbf{p}',S'M_S') = \delta_{SS'}\frac{2}{\pi}\sum_{LL'J}\sum_{M_LM_L'M_J}i^{L-L'}(S'M_S'L'M_L'|JM_J)(SM_SLM_L|JM_J)Y_{L'M_L'}(\hat{\mathbf{p}}')Y_{LM_L}^*(\hat{\mathbf{p}})\psi_{L'L}^{JST}(p',p)P_T ,$$

(2.16a)

with

$$\psi_{L'L}^{JST}(p',p) = \frac{\pi}{2}\frac{\delta(p'-p)}{p^2}\delta_{L'L} + \frac{T_{L'L}^{JST}(p',p)}{E(p',p)} ,$$

(2.16b)

one obtains

$$\langle\epsilon,\mathbf{k};\psi_{\mathbf{p}'}^{(-)S'M_S'}|V_{\text{exch}}|0;\psi_\mathbf{p}^{(+)SM_S}\rangle$$

$$= \sqrt{2\pi/k}\frac{1}{3\pi^2}\delta_{SS'}\sum i^{L''-L'}i^{L-L'''}(S'M_S'L'M_L'|J'M_J')(SM_SLM_L|JM_J)Y_{L'M_L'}(\hat{\mathbf{p}}')Y_{LM_L}^*(\hat{\mathbf{p}})$$

$$\times(-)^{S+M_J}[L''L'''JJ'][(L'''0L''0|10)\begin{bmatrix}J' & J & 1 \\ L''' & L'' & S\end{bmatrix}$$

$$\times\sum_\mu(-)^\mu\epsilon_{-\mu}(J-M_JJ'M_J'|1\mu)\delta_{T,T'\pm1}$$

$$\times\left\{\frac{\pi}{2}\left[\delta_{L'L''}\left[\frac{d}{dp'}T_{L'''L}^{JST}(p',p)-\frac{1}{2}[L''(L''+1)-L'''(L'''+1)-2]\frac{T_{L'''L}^{JST}(p',p)}{p'}\right]\right.\right.$$

$$\left.+\delta_{L'''L}\left[\frac{d}{dp}T_{L''L'}^{J'S'T'}(p,p')-\frac{1}{2}[L'''(L'''+1)-L''(L''+1)-2]\frac{T_{L''L'}^{J'S'T'}(p,p')}{p'}\right]\right]$$

$$+\int_0^\infty dp''p''\left[p''\left[\frac{T_{L''L'}^{J'S'T'}(p,p')}{E(p'',p')}\frac{d}{dp''}T_{L'''L}^{JST}(p'',p)+\frac{T_{L'''L}^{JST}(p'',p)}{E(p'',p)}\frac{d}{dp''}T_{L''L'}^{J'S'T'}(p'',p')\right]\right.$$

$$\left.-\frac{1}{2}\left[\frac{L''(L''+1)-L'''(L'''+1)-2}{E(p'',p')}+\frac{L'''(L'''+1)-L''(L''+1)-2}{E(p'',p)}\right]\right.$$

$$\left.\left.\times T_{L''L'}^{J'S'T'}(p'',p')T_{L'''L}^{JST}(p'',p)\right]\right\} ,$$

(2.17)

where Eq. (2.11) has been used. Since all the T-matrix elements involved in the above equation have the same boundary condition $(+)$, we have also dropped the superscript $+$ for simplicity. Therefore $T_{L'L}^{JST}(p',p)$ should be understood as $T_{L'L}^{JST^+}(p',p)$ in the above equation. The summation in Eq. (2.17) runs over T, T', J, J', M_J, M_J', all L's, and their corresponding projection M_L's.

If the incident beam and target are unpolarized and the final state spins and photon polarization are unobserved, the NN bremsstrahlung cross section is given by[20]

$$d\sigma = \frac{\left\{\frac{1}{4}\sum_{\substack{SS' \\ M_S M_S'}}\sum_{\epsilon}|(\epsilon_1'\epsilon_2'\omega)^{1/2}\langle \epsilon, \mathbf{k}; \mathbf{p}_1'\mathbf{p}_2'S'M_S'|V_{\text{em}}|0; \mathbf{p}_1\mathbf{p}_2 S M_S\rangle\sqrt{\epsilon_1\epsilon_2}|^2\right\}}{\{\epsilon_1\epsilon_2[(\boldsymbol{\beta}_1-\boldsymbol{\beta}_2)^2-(\boldsymbol{\beta}_1\Lambda\boldsymbol{\beta}_2)^2]^{1/2}\}}$$
$$\times \left\{(2\pi)^4\delta^3(\mathbf{p}_1+\mathbf{p}_2-\mathbf{p}_1'-\mathbf{p}_2'-\mathbf{k})\delta(\epsilon_1+\epsilon_2-\epsilon_1'-\epsilon_2'-\omega)\frac{d^3p_1'}{(2\pi)^3\epsilon_1'}\frac{d^3p_2'}{(2\pi)^3\epsilon_2'}\frac{d^3k}{(2\pi)^3\omega}\right\}, \tag{2.18}$$

where ω denotes the energy of the photon with momentum $\mathbf{k}$ and $\boldsymbol{\beta}_i \equiv \mathbf{p}_i/\epsilon_i$. The primed (unprimed) quantities correspond to the final (initial) nucleons' energies ϵ_1',ϵ_2' (ϵ_1,ϵ_2), and momenta $\mathbf{p}_1',\mathbf{p}_2'$ $(\mathbf{p}_1,\mathbf{p}_2)$, which are related to the final (initial) relative momentum $\mathbf{p}'$ $(\mathbf{p})$ by

$$\mathbf{p}_1' = \frac{\mathbf{P}}{2}+\mathbf{p}'-\frac{\mathbf{k}}{2},$$
$$\mathbf{p}_2' = \frac{\mathbf{P}}{2}-\mathbf{p}'-\frac{\mathbf{k}}{2}, \tag{2.19a}$$

and

$$\mathbf{p}_1 = \frac{\mathbf{P}}{2}+\mathbf{p},$$
$$\mathbf{p}_2 = \frac{\mathbf{P}}{2}-\mathbf{p}, \tag{2.19b}$$

with $\mathbf{P}$ denoting the initial NN c.m. momentum. Each term enclosed in curly brackets in Eq. (2.18) is a Lorentz invariant and may be evaluated in any convenient Lorentz frame.

A quantity of particular interest is the photon cross section per unit photon energy and per unit photon solid angle

$$\frac{d^2\sigma}{d\omega d\Omega} = \frac{2\pi\omega}{\{\epsilon_1\epsilon_2[(\boldsymbol{\beta}_1-\boldsymbol{\beta}_2)^2-(\boldsymbol{\beta}_1\Lambda\boldsymbol{\beta}_2)^2]^{1/2}\}}$$
$$\times \int \frac{d^3p_1'}{(2\pi)^3\epsilon_1'}\frac{d^3p_2'}{(2\pi)^3\epsilon_2'}\left\{\frac{1}{4}\sum_{\substack{SS' \\ M_S M_S'}}\sum_{\epsilon}|(\epsilon_1'\epsilon_2'\omega)^{1/2}\langle \epsilon, \mathbf{k}; \mathbf{p}_1'\mathbf{p}_2'S'M_S'|V_{\text{em}}|0; \mathbf{p}_1\mathbf{p}_2 S M_S\rangle\sqrt{\epsilon_1\epsilon_2}|^2\right\}$$
$$\times\delta(\epsilon_1'+\epsilon_2'+\omega-\epsilon_1-\epsilon_2)\delta^3(\mathbf{p}_1'+\mathbf{p}_2'+\mathbf{k}-\mathbf{p}_1-\mathbf{p}_2). \tag{2.20}$$

The above quantity is most easily expressed in the final NN c.m. frame

$$\frac{d^2\sigma}{d\omega d\Omega} = \frac{1}{\{\epsilon_1\epsilon_2[(\boldsymbol{\beta}_1-\boldsymbol{\beta}_2)^2-(\boldsymbol{\beta}_1\Lambda\boldsymbol{\beta}_2)^2]^{1/2}\}}\frac{\omega}{(2\pi)^5}$$
$$\times \int d\Omega'\left[\frac{p'}{2\epsilon_{p'}}\right]\left\{\frac{1}{4}\sum_{\substack{SS' \\ M_S M_S'}}\sum_{\epsilon'}|(\epsilon_1'\epsilon_2'\omega)^{1/2}\langle \epsilon, \mathbf{k}; \mathbf{p}_1'\mathbf{p}_2'S'M_S'|V_{\text{em}}|0; \mathbf{p}_1\mathbf{p}_2 S M_S\rangle\sqrt{\epsilon_1\epsilon_2}|^2\right\}. \tag{2.21}$$

Again, the terms in curly brackets are evaluated in convenient frames, as they are Lorentz invariants.

The transformation of the cross section from one frame to another is given by

$$\frac{d\sigma}{d\omega'd\Omega'} = \frac{\omega'}{\omega}\frac{d\sigma}{d\omega d\Omega}. \tag{2.22}$$

III. RESULTS FOR NEUTRON-PROTON BREMSSTRAHLUNG

Since for photon energies of interest (<150 MeV) np bremsstrahlung is the dominant reaction for photon production among collisions involving different species of nucleons, we will consider only this process. In the elec-

tromagnetic dipole approximation the proton-proton (pp) and neutron-neutron (nn) photon emission amplitudes vanish identically. We will discuss pp bremsstrahlung and its influence on the production of high-energy photons in proton-nucleus as well as in nucleus-nucleus collisions in a future work.

In the present work we have used one of the recent one-boson-exchange potentials developed by the Bonn group,[21] hereafter denoted by HM86. The T-matrix elements have been generated as described in Ref. 22. Two-nucleon states up to $J=6$ have been included.

In Table I the np bremsstrahlung cross section $d^2\sigma/d\Omega_n d\Omega_p$ in the coplanar geometry is shown at a neutron incident energy of $T_{lab}=200$ MeV and for several final state neutron and proton angles, θ_n and θ_p. A comparison of the present results (fifth column) with the experimental data (last column) shows good agreement for $\theta_n=\theta_p=30°$ and $35°$. Although the experimental uncertainties are large at larger angles the present calculation underpredicts the data. Due to the scarcity of np bremsstrahlung data, it is not possible to test in detail how the present approach works. A similar feature shown by our results is also observed in an earlier calculation,[15] whose results are also displayed in the third and fourth columns. The essential differences between these two calculations are that in the present work we have neglected the rescattering contribution due to the one-body current term and have used a different NN potential. In Fig. 1, we show a comparison between our results and those of Ref. 15 for the cross section $d^3\sigma/d\Omega_p d\Omega_n d\theta$, where the contribution from the external radiation is isolated. The integration of this cross section over the photon emission angle θ yields the result shown in the last row of Table I. As one sees, there is an appreciable difference in the external radiation contribution between the two calculations. Since the external radiation is due to the one-body current contribution except for the rescattering term, one concludes that the differences in the results of Table I between the two calculations are partly due to the different NN potentials used. The structure exhibited by the cross section in Fig. 1 can be easily understood if we remember that photons are emitted primarily in the direction perpendicular to the velocity of the scattered proton.

TABLE I. The coplanar $np\gamma$ cross section $d^2\sigma/d\Omega_n d\Omega_p$ in μb/sr^2 for incident laboratory energy $T_{lab}=200$ MeV and various neutron and proton exit angles θ_n and θ_p, in degrees. The present results for the HM86 potential are in the column denoted HM86, while the results of Ref. 15 for the Bryan-Scott (BS) and Hamada-Johnston (HJ) potentials are in the third and fourth columns. The experimental data in the last column are from Ref. 23.

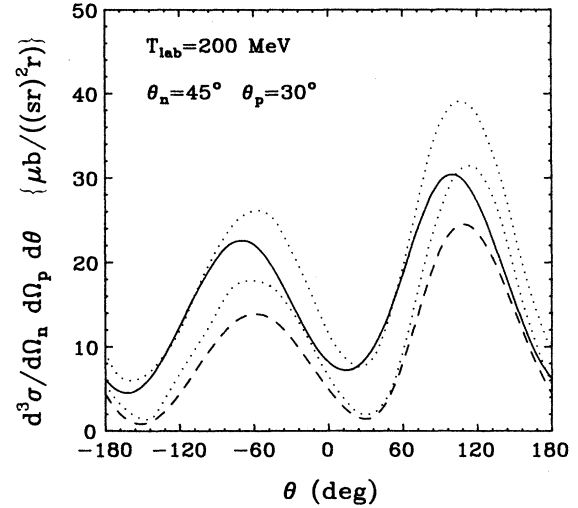| θ_n	θ_p	BS	HJ	HM86	Expt.
30	30	34.1	34.6	34.8	35±14
35	35	44.7	44.0	43.1	57±13
38	38	71.4	69.8	64.9	116±20
40	30	72.0	69.9	58.8	114±44
45	30	128.0	121.0	94.2	132±53

FIG. 1. The coplanar $np\gamma$ cross section $d^3\sigma/d\Omega_n d\Omega_p d\theta$ with incident energy $T_{lab}=200$ MeV for $\theta_n=45°$ and $\theta_p=30°$. The dashed line is the contribution from external radiation, while the solid curve includes both internal and external radiations. The dotted curves are the corresponding results from Ref. 15 for the Hamada-Johnston potential.

In Figs. 2(a) and (b) a comparison between our results and those of Ref. 13 are shown for the angle integrated differential cross section $d\sigma/d\omega$ multiplied by the photon energy ω at the NN c.m. energies $T_{c.m.}=50$ and 200 MeV. As one can see, the two results practically agree with each other for the $T_{c.m.}=50$ MeV case, but for $T_{c.m.}=200$ MeV, our result is smaller than that of Ref. 13 by $\sim 25\%$ in the very high photon energy region. Again this difference may in part be due to the different NN potential used. However, in contrast to the case of Fig. 1, the discrepancy here might largely be due to our omission of the rescattering contribution from the one-body current, since in this case it involves much higher photon energies than in the case of Fig. 1.

Figures 3(a) and (b) show the double differential cross section $d^2\sigma/d\omega d\Omega$ at $T_{lab}=150$ and 300 MeV for photon emission angle of $\theta=30°$. Here, we separate the contributions from the different parts of the current, i.e., the convection, the magnetization, and the two-body current. The latter is mainly the meson-exchange current.[15] As one sees, for small photon energies the convection current dominates, where contribution to the bremsstrahlung cross section goes as $1/\omega$. The deviation from $1/\omega$ behavior as ω increases is mainly due to the momentum dependence of the T matrix. For $\omega \gtrsim 50$ MeV, the two-body current starts to dominate, so the higher-energy photons come mainly from this mechanism. The ω dependence of the two-body current contribution can be easily understood since it is dominated by the one-pion-exchange current [see Eqs. (3.1) and (3.3)]. The later contribution in the Born approximation is shown in Fig. 4. Although smaller than the meson-exchange current in the high-energy region, the magnetization current becomes comparable to or even larger than the convection current. Indeed, for extremely high photon energies the

magnetization current dominates over other currents.[1] We observe that in contrast to the convection current contribution which goes as $1/\omega$, the magnetization current contribution goes as ω in the low-energy limit. The deviation from the linear dependence is again largely due to the momentum dependence of the T matrix. Although the one-body current contribution itself is smaller than the two-body current contribution, its interference with the latter is very important and increases the photon cross section (constructive interference). The total contribution is then a very flat function of ω. An interesting feature exhibited by the pn bremsstrahlung cross section is that it increases rather rapidly as ω approaches its maximum allowed value and only drops at the very end point. As one can see, this increase is due to the one-body current contribution.

The two-body current contribution, which is the dom-

inant process in the high photon energy region, is calculated in the limit of $k \to 0$. Therefore, one might question the validity of such an approximation, and consequently the results discussed before, where the photon reaches an energy as high as 140 MeV. The two-body current contribution is dominated by the one-pion exchange current. In Ref. 18 the validity of the $k \to 0$ approximation has been checked for the one-pion-exchange potential, where a full calculation can be performed. They found the $k \to 0$ approximation to be a good one even for photon energies as high as 100 MeV. Since the calculation of Ref. 18 involved very special kinematics, we have made a rough check of the validity of the approximation for conditions of interest to us.

The one-pion exchange contribution to the $pn\gamma$ emission amplitude in the Born approximation can be calculated directly from the Feynman diagram giving[15]

$$\langle \epsilon, \mathbf{k}; \mathbf{p}'S'M_S'T' | V_{\text{exch}}^{\text{ope}} | 0; \mathbf{p}SM_S T \rangle = -2e\sqrt{2\pi/k} \left[\frac{f_\pi}{\mu_\pi} \right]^2 \left\langle T', M_T'=0 \left| \frac{i}{2}(\tau_1 \Lambda \tau_2)_z \right| T, M_T=0 \right\rangle$$

$$\times \left[2 \frac{\epsilon \cdot \mathbf{q} \langle S'M_S' | \sigma_1 \cdot \mathbf{q}_- \sigma_2 \cdot \mathbf{q}_+ | SM_S \rangle}{(q_-^2 + \mu_\pi^2)(q_+^2 + \mu_\pi^2)} - \frac{\langle S'M_S' | \sigma_1 \cdot \epsilon \sigma_2 \cdot \mathbf{q}_+ | SM_S \rangle}{q_+^2 + \mu_\pi^2} \right.$$

$$\left. - \frac{\langle S'M_S' | \sigma_1 \cdot \mathbf{q}_- \sigma_2 \cdot \epsilon | SM_S \rangle}{q_-^2 + \mu_\pi^2} \right]. \tag{3.1}$$

Here, $(f_\pi^2/4\pi)=0.08$ is the square of the dimensionless $NN\pi$ coupling strength and $\mu_\pi=0.7$ fm^{-1} denotes the pion mass; the momentum transfers $\mathbf{q}$ and $\mathbf{q}_+$ and $\mathbf{q}_-$ are defined as

$$\mathbf{q} \equiv \mathbf{p}' - \mathbf{p}, \tag{3.2a}$$

and

$$\mathbf{q}_\pm \equiv \mathbf{q} \pm \frac{\mathbf{k}}{2}. \tag{3.2b}$$

The isospin matrix element in Eq. (3.1) yields $+1$ or -1 according to $T=0$, $T'=1$ or $T=1$, $T'=0$ and zero otherwise. In the soft-photon limit Eq. (3.1) reduces to

$$\langle \epsilon, \mathbf{k}; \mathbf{p}'S'M_S'I' | V_{\text{exch}}^{\text{ope}} | 0; \mathbf{p}SM_S T \rangle = -2e\sqrt{2\pi/k} \left[\frac{f_\pi}{\mu_\pi} \right]^2 \left\langle T', M_T'=0 \left| \frac{i}{2}(\tau_1 \Lambda \tau_2)_z \right| T, M_T=0 \right\rangle$$

$$\times \left[2 \frac{\epsilon \cdot \mathbf{q} \langle S'M_S' | \sigma_1 \cdot \mathbf{q} \sigma_2 \cdot \mathbf{q} | SM_S \rangle}{(q^2 + \mu_\pi^2)^2} \right.$$

$$\left. - \frac{\langle S'M_S' | (\sigma_1 \cdot \epsilon \sigma_2 \cdot \mathbf{q} + \sigma_1 \cdot \mathbf{q} \sigma_2 \cdot \epsilon) | SM_S \rangle}{q^2 + \mu_\pi^2} \right], \tag{3.3}$$

which can be obtained also from Eq. (2.6) if one replaces there $V(\mathbf{p}',\mathbf{p})$ by the one-pion-exchange potential.

In Fig. 4, a comparison of the double differential cross section is shown for the one-pion-exchange current contribution in the Born approximation in the full calculation (solid curve) and the $k \to 0$ approximation (dashed curve). As one sees, both results are almost identical over the range of ω allowed kinematically at $T_{\text{c.m.}}=200$ MeV.

We now analyze in detail some of the aspects of the pn bremsstrahlung cross section. In Figs. 5(a)–(d) we show again the differential cross section at $T_{\text{lab}}=150$ MeV for

the convection, magnetization, two-body, and total contributions, respectively. The solid curves are the results of the full calculation as shown in Fig. 3(a). They are plotted again here basically for the sake of comparison. As mentioned before, an interesting feature exhibited by the pn bremsstrahlung cross section is the enhancement observed as ω approaches its maximum kinematically allowed value. One might argue that this is due to the fact that it is approaching the quasideuteron ($^1S_0$) resonance, since the final neutron and proton velocities approach zero as ω approaches its maximum. The dashed curves

are the results when the $^1S_0$ state is switched off. As one can see, the $^1S_0$ state has very little influence on the cross section which still exhibits the same feature as the full calculation. The difference appears only at the very end point ($\omega \gtrsim 70$ MeV) where the cross section is reduced by a factor ~ 2. In the case of Fig. 5 the starting energy corresponding to $\omega = 70$ MeV (where the cross section peaks) is ~ 2.2 MeV which is still relatively far from the singlet deuteron resonance located at 0.08 MeV. In fact, this resonance value is only reached at $\omega \simeq 72$ MeV.

The dotted curves are the results when the $^3(SD)_1$ contribution from the full calculation is switched off. As one can see, the cross section is strongly reduced, especially at high energies. Note also the effect of the interference at the very end point. This strong sensitivity of the photon cross section can be attributed in part to strong short-range correlations present in the $^3S_1$ state, which make the resulting T matrix roughly twice as attractive as in the $^1S_0$ state.[24] This result combined with the spin statistical factor increases the contribution of the $^3S_1$ state on the cross section by an order of magnitude compared to the $^1S_0$ state. For the meson-exchange contribution the reduction reaches nearly an order of magnitude. Since the $^3S_1$ state is the one most sensitive to the short-range correlations, the $np\gamma$ reaction may offer a good tool for investigating short-range correlation effects.

Finally, the dash-dotted curves in Fig. 5 are the results when the T-matrix elements are all forced to be on the energy shell, so the difference between these and the solid curves is due to off-energy-shell effects. As one sees, the convection and magnetization current contributions are now reduced with respect to the full results especially at

high photon energies. In particular, we do not observe the rapid rising of the cross section as in the full calculation at high ω. However, for the meson-exchange contribution the effect is just the opposite so the cross section is enhanced at high ω. As a result the off-energy-shell effect has practically no net influence on the pn bremsstrahlung inclusive cross section. However, in the case of pp bremsstrahlung the off-energy-shell effect might be considerable since the meson-exchange current does not contribute in that case. Therefore, pp bremsstrahlung with high-energy photons may offer a real possibility of studying the off-energy-shell behavior of the T matrix.[25,26]

IV. NUCLEON-NUCLEUS BREMSSTRAHLUNG

As in Ref. 12 we consider only the first chance collision to calculate the bremsstrahlung rate since we are interested in high-energy photons and write the probability of photon emission per unit solid angle and unit photon energy as

$$\frac{d^2P}{d\omega\,d\Omega} = \frac{1}{W_{NN}}\frac{d^2W_{pn\gamma}}{d\omega\,d\Omega} \ , \tag{4.1}$$

where $d^2W_{pn\gamma}/d\omega\,d\Omega$ stands for the nucleon-nucleus bremsstrahlung differential transition rate and W_{NN} the total NN collisional rate irrespective of the bremsstrahlung. We calculate these quantities in the nuclear matter approximation.

The nucleon-nucleus bremsstrahlung transition rate is obtained by integrating the NN bremsstrahlung rate over the Fermi distribution of the target nucleus characterized by the Fermi momentum k_f:
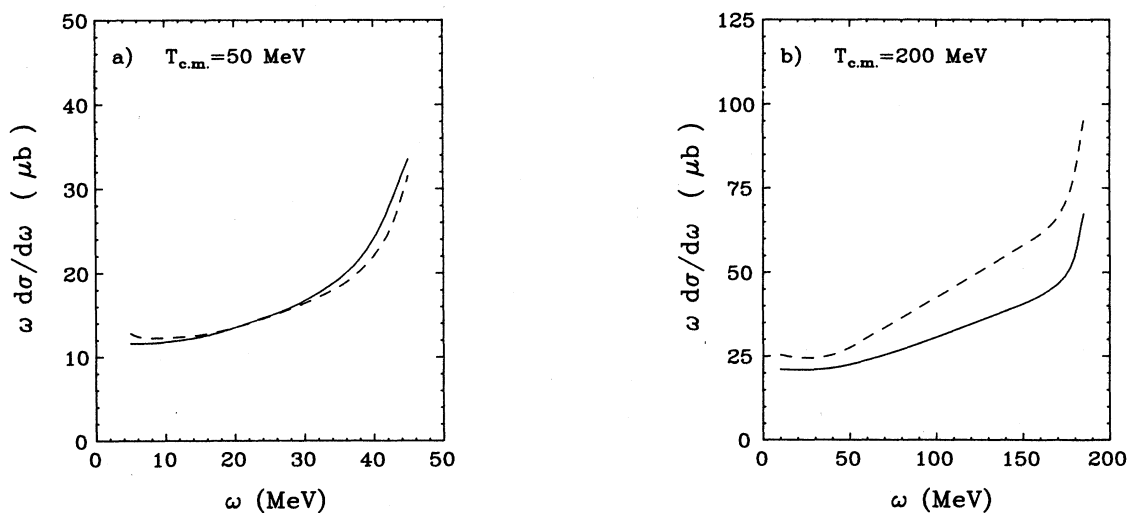

FIG. 2. The $np\gamma$ cross section $d\sigma/d\omega$ multiplied by the photon energy ω in the initial neutron-proton center-of-mass frame at the center-of-mass energy $T_{c.m.} = 50$ MeV (a) and 200 MeV (b). The solid curves are the results of the present calculation using the HM86 potential, while the dashed curves correspond to those from Ref. 13 with the Reid-soft-core potential.
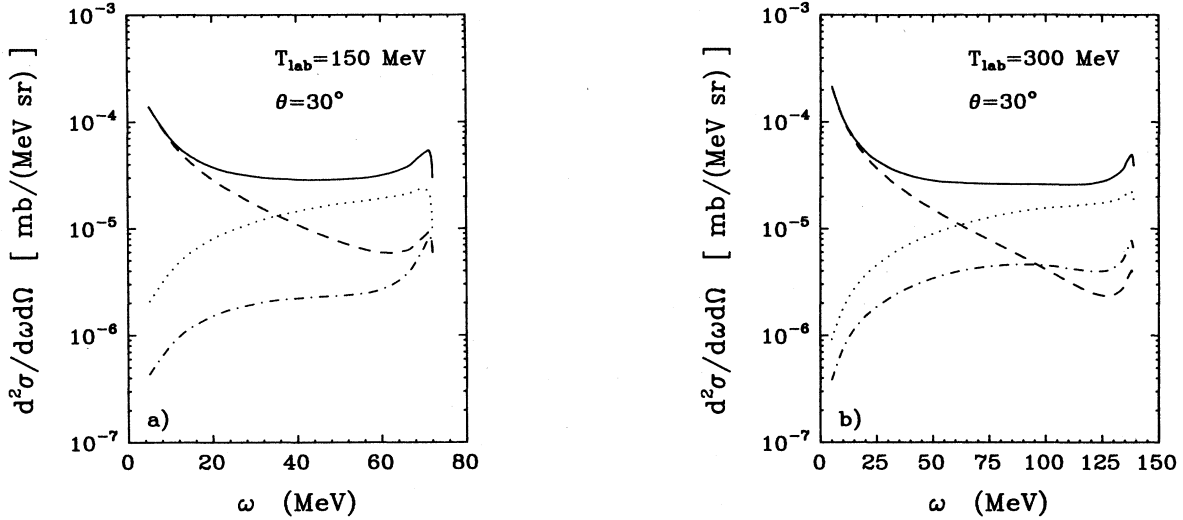
FIG. 3. The differential $pn\gamma$ cross section $d^2\sigma/d\omega\,d\Omega$ in the initial proton-neutron center-of-mass frame as a function of the photon energy ω for the photon emission angle $\theta=30°$. The incident energies are $T_{\text{lab}}=150$ MeV (a) and 300 MeV (b). The dot-dashed curves are the contributions from the magnetization current, the dotted lines from the two-body current, and the dashed ones from the convection current. The solid curves are the corresponding total contributions.

$$\frac{d^2W_{pn\gamma}}{d\omega\,d\Omega} = \frac{1}{\varepsilon_1}\int_{<k_f}\frac{d^3p_2}{(2\pi)^3\varepsilon_2}2\pi\omega\int\frac{d^3p_1'}{(2\pi)^3\varepsilon_1'}\frac{d^3p_2'}{(2\pi)^3\varepsilon_2'}Q$$

$$\times\left[\frac{1}{4}\sum_{\substack{SS'\\M_SM_S'}}\sum_{\epsilon}|(\varepsilon_1'\varepsilon_2'\omega)^{1/2}\langle\epsilon,\mathbf{k};\mathbf{p}_1'\mathbf{p}_2'S'M_S'|V_{\text{em}}|0;\mathbf{p}_1\mathbf{p}_2SM_S\rangle\sqrt{\varepsilon_1\varepsilon_2}|^2\right]$$

$$\times\delta^3(\mathbf{p}_1+\mathbf{p}_2-\mathbf{k}-\mathbf{p}_1'-\mathbf{p}_2')\delta(\varepsilon_1+\varepsilon_2-\varepsilon_1'-\varepsilon_2'-\omega)\ . \tag{4.2}$$

Here the Pauli blocking operator Q excludes the target Fermi sphere. In the nuclear matter rest frame

$$Q=\theta(p_1'-k_f)\theta(p_2'-k_f)\ . \tag{4.3}$$

Similar to the nucleon-nucleus bremsstrahlung rate, the total NN collisional rate is obtained as

$$W_{\text{NN}}=\frac{1}{\varepsilon_1}\int_{<k_f}\frac{d^3p_2}{(2\pi)^3\varepsilon_2}\int\frac{d^3p_1'}{(2\pi)^3\varepsilon_1'}\frac{d^3p_2'}{(2\pi)^3\varepsilon_2'}Q\left[\frac{1}{4}\sum_{\substack{SS'\\M_SM_S'}}|(\varepsilon_1'\varepsilon_2')^{1/2}\langle\mathbf{p}_1'\mathbf{p}_2'S'M_S'|G|\mathbf{p}_1\mathbf{p}_2SM_S\rangle\sqrt{\varepsilon_1\varepsilon_2}|^2\right]$$

$$\times(2\pi)^4\delta^3(\mathbf{p}_1+\mathbf{p}_2-\mathbf{p}_1'-\mathbf{p}_2')\delta(\varepsilon_1+\varepsilon_2-\varepsilon_1'-\varepsilon_2')\ , \tag{4.4}$$

where G denotes the G matrix.

In Eqs. (4.2) and (4.4), in contrast to the free NN case, the single-particle energies ε_i contain, in addition to the kinetic energy, the potential energy due to the mean field of the target nucleus. The Pauli blocking and the mean field potential not only affect the initial and final states but also the intermediate states [see Eq. (2.3)]. In particular one should use the G matrix instead of the T matrix throughout.

The G-matrix elements are calculated according to Ref. 22 and the corresponding mean field potential is generated within the Brueckner-Hartree-Fock approximation in nuclear matter using the so-called continuous choice.[27]

The bremsstrahlung cross section is obtained simply by multiplying the probability rate given in Eq. (4.1) by the cross-sectional area of the target

$$\frac{d^2\sigma}{d\omega\,d\Omega}=\pi R^2\frac{d^2P}{d\omega\,d\Omega}\ , \tag{4.5}$$

where R is the radius of the target nucleus.

V. RESULTS FOR PROTON-NUCLEUS BREMSSTRAHLUNG

In Fig. 6 we show results for the probability rate at a proton incident energy of $T_{\text{lab}}=140$ MeV and for a photon emission angle $\theta=90°$. The Fermi momentum is $k_f=1.36$ fm^{-1}. As one sees, the probability rate exhibits a feature similar to the pn bremsstrahlung. Due to the

relatively large meson-exchange contribution in the high photon energy region the total probability rate is rather flat as a function of ω. However, due to the Pauli blocking effect, we no longer observe the increase of the cross section at high energies as in the case of the pn bremsstrahlung.

In Fig. 6, results using the T-matrix elements are also shown. We emphasize that the only difference from the G-matrix results is in the *nuclear matrix elements* keeping all other quantities unchanged. One can see that there is only a small difference between the G- and T-matrix results, showing that the Pauli blocking and the mean field potential in the *intermediate* states have a minor effect on the bremsstrahlung cross section. Since the G matrix used corresponds to nuclear matter normal density, the difference shown in Fig. 6 may be considered as an upper limit.

In Fig. 7 we show the sensitivity of the photon probability rate on the nuclear matter density and the corresponding mean field potential in the initial and final states. Here we have used the T matrix for the nuclear matrix elements in view of the results shown in Fig. 6. When the density is reduced to $\sim 10\%$ of normal density ($k_f = 0.65$ fm^{-1}), one obtains the results shown as the dashed line. Comparing to the full density result (solid curve), one sees that it is steeper. In the low photon energy region the bremsstrahlung transition rate increases with respect to the full density case, since there is more phase space available for a small Fermi sphere. On the other hand, due to the deeper mean field potential for larger densities the nucleon moves faster and consequently the photon emission amplitude becomes larger as the density increases. The competition between these two effects determines the magnitude of the bremsstrahlung cross section. In the present case, the availability of phase space dominates. Unlike the case at larger Fermi momentum, in the high-energy region there is no energy available to make energetic photons. Therefore the slope of the transition rate becomes much steeper as the density decreases. Indeed, at $T_{lab} = 140$ MeV incident energy and with the nuclear matter self-consistent mean field potential used here the maximum photon energy allowed is $\omega_{max} \simeq 167$ and 150 MeV for $k_f = 1.36$ and 0.65 fm^{-1}, respectively. These relatively large values of ω_{max} are a consequence of the deep mean field potential obtained in the Brueckner-Hartree-Fock calculation in nuclear matter. In fact, at $k_f = 1.36$ fm^{-1} the single-particle potential on the Fermi surface is still as deep as -64 MeV, while at $k_f = 0.65$ fm^{-1} it is about -20 MeV. (The nuclear matter mean field potential may be too unrealistic for finite nuclei.) For the same reason the NN collisional rate also increases as density decreases, and since the probability rate is the ratio between the transition rate and the total collisional rate, the result is what we see in Fig. 7.

The dash-dotted curve in Fig. 7 is the result at $k_f = 1.36$ fm^{-1} in an extreme situation when the mean field potential is completely switched off; this shows the sensitivity of the probability rate on the mean field potential in the initial and final state. One sees that in the high-energy region it reduces the rate by more than an
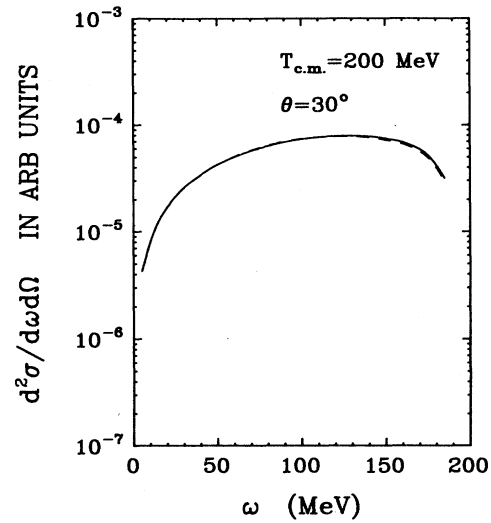

FIG. 4. The one-pion-exchange contribution to the $pn\gamma$ cross section $d^2\sigma/d\omega\,d\Omega$ (in arbitrary units) in the initial proton-neutron center-of-mass frame at the center-of-mass energy $T_{c.m.} = 200$ MeV and for the photon emission angle $\theta = 30°$. The results are obtained in the Born approximation. The solid curve is the full calculation using Eq. (3.1), while the dashed one is the $\mathbf{k} \rightarrow 0$ approximation [Eq. (3.3)]. There is practically no difference between these two calculations on this scale.

order of magnitude (compare with the solid curve). This drastic sensitivity is due to the fact that there is much less phase space available to make energetic photons when the mean field is set to zero. In fact, $\omega_{max} \simeq 103$ MeV in this case. The dotted curve is the corresponding result at $k_f = 0.65$ fm^{-1}. In this case, one has $\omega_{max} \simeq 130$ MeV which explains the larger probability rate for high photon energies than the former case.

Finally, in Fig. 8, we show the comparison between our result and the experimental data for the bremsstrahlung cross section for $p + {}^9$Be at $T_{lab} = 140$ MeV and $\theta = 90°$. Although our result corresponds to the probability rate calculated in the extreme situation of $k_f = 1.36$ fm^{-1} and no mean field potential (dash-dotted line in Fig. 7) the agreement is reasonable. (We remember that under these conditions the maximum photon energy allowed is $\omega_{max} \simeq 103$ MeV.) However, since the proton-nucleus bremsstrahlung cross section is very sensitive to the density of the nucleus, a more realistic calculation than that reported here seems necessary.

VI. CONCLUSION

We have investigated the role of the NN collisional mechanism in producing energetic photons in the np reaction as well as in proton-induced reactions at intermediate bombarding energies. The formulation of the underlying dynamics is basically that of Brown and Franklin[15] which fulfills the gauge invariance requirements. The present calculations have been carried out using a very recent version of the one-boson-exchange potential developed by the Bonn group.[21] The present calculation yields np bremsstrahlung cross sections which

exhibit the same general feature of those obtained by Brown and Franklin[15] and by Neuhauser and Koonin,[13] although there are differences in details as have been discussed.

The role of the different parts of the current on the photon cross section has been investigated. We have seen that low-energy photons ($\omega \lesssim 20$ MeV) arise primarily from the convection current, while higher-energy photons ($\omega \gtrsim 50$ MeV) are predominantly from the meson-exchange current. For $20 \lesssim \omega \lesssim 50$ MeV there is competition between these two current contributions. The magnetization current contribution is not a dominant one in the region of photon energy investigated; however, it becomes larger than the convection current contribution

for $\omega \gtrsim 100$ MeV. The interferences between these currents are constructive and play an important role in enhancing the cross section. As a result, the total contribution exhibits a cross section which is quite flat as a function of photon energy. Unfortunately, due to the scarcity of the experimental data on np bremsstrahlung, detailed tests of the theory are not yet possible. Undoubtedly, more data are required, especially as a function of photon energy, in order to understand better the underlying dynamics.

If we assume the theory to be "correct" then the np bremsstrahlung reaction might be used as a tool to study NN short-range correlations since the photon cross section is extremely sensitive to the $^3(SD)_1$ states, especially
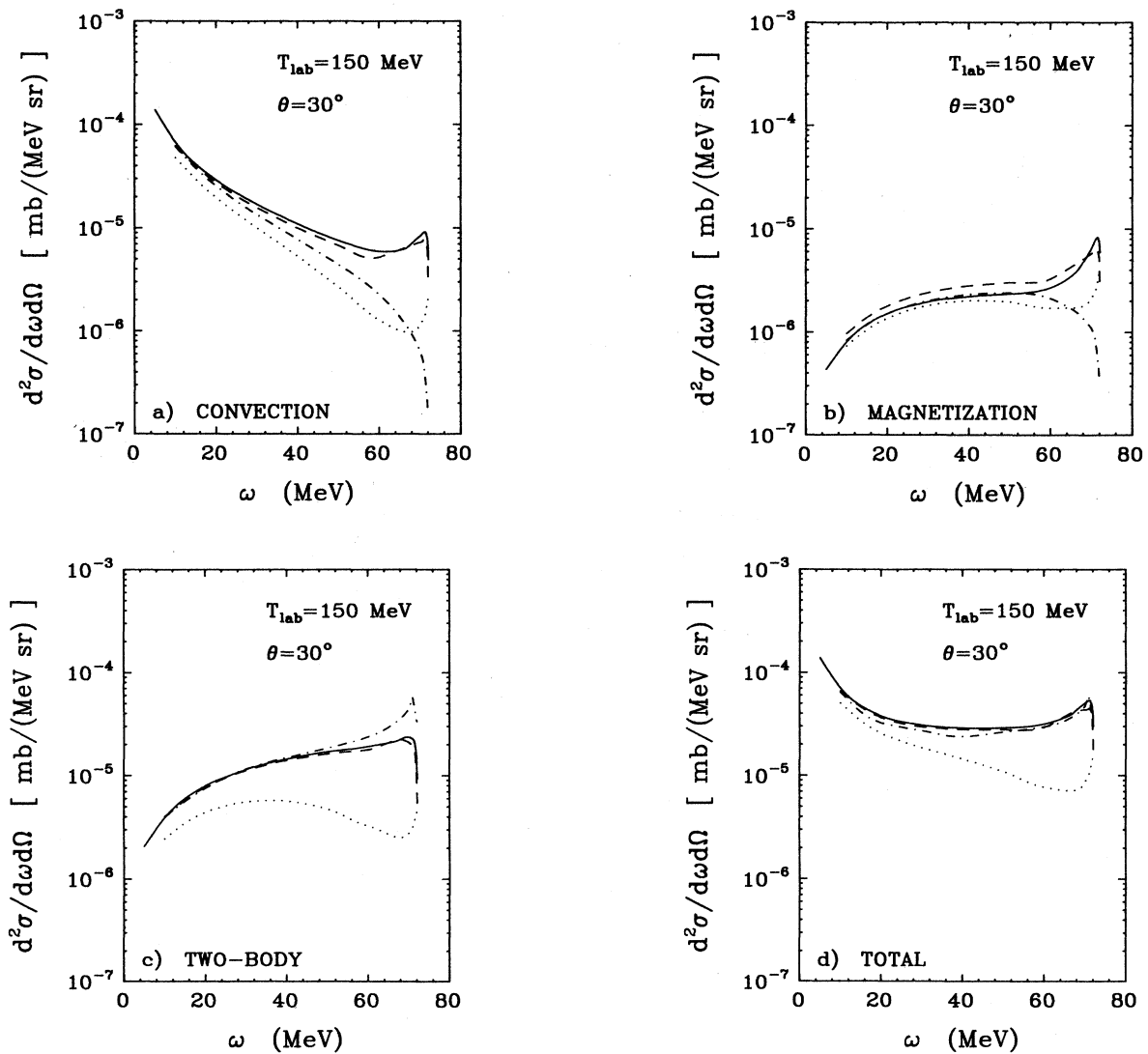

FIG. 5. The $pn\gamma$ cross section $d^2\sigma/d\omega\,d\Omega$ in the initial proton-neutron center-of-mass frame at $T_{lab} = 150$ MeV and for the photon emission angle $\theta = 30°$. (a), (b), (c), and (d) correspond to the convection current, magnetization current, two-body current, and total contributions, respectively. The dashed curves are the results when the $^1S_0$ state is excluded; the dotted lines are when the $^3(SD)_1$ states are excluded and the dot-dashed ones correspond to the results using the T-matrix elements on the energy shell. The solid curves correspond to the full calculation.
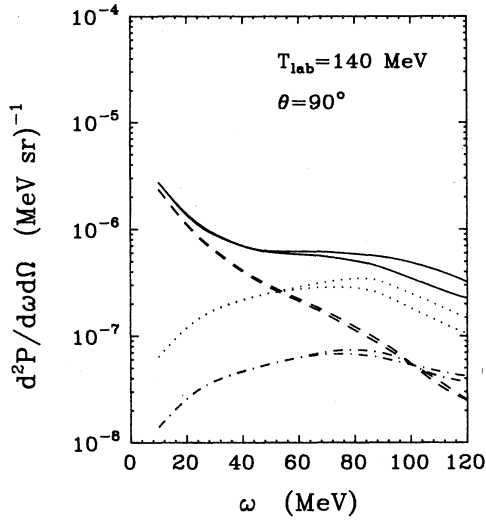
FIG. 6. The differential photon emission probability rate in the laboratory frame for proton-nucleus-induced reaction at the incident energy $T_{lab} = 140$ MeV and the photon emission angle $\theta = 90°$. The dot-dashed curves correspond to the magnetization current contribution, the dotted lines to the two-body current, and the dashed ones to the convection current. The solid curves are the total contributions. The curves corresponding to the different currents and yielding larger cross sections are the results using the G matrix, while those of smaller cross sections correspond to the T-matrix results. The Fermi momentum is $k_f = 1.36$ fm^{-1}.

FIG. 8. A comparison between the present results and the experimental data from Ref. 28 for the proton-nucleus bremsstrahlung cross section at the incident energy $T_{lab} = 140$ MeV and for photon emission angle $\theta = 90°$. The curve corresponds to our result at $k_f = 1.36$ fm^{-1} using a zero mean field potential and the T matrix.

at high photon energies.

We have also investigated off-energy-shell effects of the T matrix. For the one-body current contribution the off-energy-shell effect enhances considerably the photon cross section in the high photon energy region, while for the two-body current contribution it reduces the cross section. The final result is that the np bremsstrahlung inclusive cross section seems to be rather insensitive to off-energy-shell effects, although this might not be the case for exclusive cross sections. However, in the pp bremsstrahlung reaction one may be able to study the off-energy-shell effect, since in this case the two-body current is mostly absent. Of course, the convection current contribution is also suppressed to a large extent relative to the np case. The study of off-energy-shell effects using pp bremsstrahlung has regained attention[25,26] with the development of accelerators of higher-energy proton beams and more sophisticated NN potentials than were available in the past.

The proton-nucleus bremsstrahlung has been studied in the nuclear matter approximation by taking into account only the first chance collision. The result for the cross section shows basically a similar feature to that of pn bremsstrahlung. The use of the G matrix or the T matrix for the nuclear matrix elements has little influence on the photon cross section, showing that the Pauli blocking and the mean field potential in the intermediate states are not so important.

However, the photon cross section seems to be extremely sensitive to Pauli blocking and the mean field potential in the initial and final states, especially for high-energy photons since for these photons the final state phase space distribution is critical.

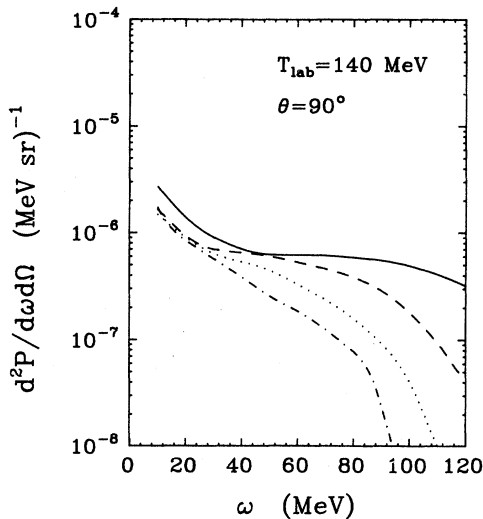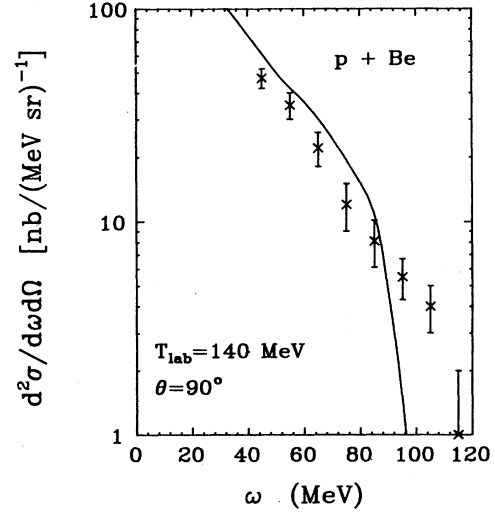Finally, the result of the present calculation of the proton-nucleus bremsstrahlung can only account for the

FIG. 7. The proton-nucleus bremsstrahlung probability rate in the laboratory system at the incident energy $T_{lab} = 140$ MeV and photon emission angle $\theta = 90°$. The dot-dashed line is the result at $k_f = 1.36$ fm^{-1} and no mean field potential, while the dotted curve corresponds to $k_f = 0.65$ fm^{-1} and no mean field potential. The solid and dashed curves are the full results for $k_f = 1.36$ and 0.65 fm^{-1}, respectively. The T matrix has been used here.

existing data under the extreme condition of $k_f = 1.36$ fm^{-1} and no mean field potential. A better calculation than the simple nuclear matter approximation calculation seems to be required in order to really pin down whether the problem is due to the artifact of the nuclear matter approximation or due to the inadequacy of the theory in describing the dynamics of the elementary process.

Finally, we have to stress that the present calculation does not include the rescattering term from the one-body current contribution. A part of this term is shown to cancel precisely the two-body current contribution in the soft-photon limit.[19] We have neglected this rescattering term based on the results of Brown and Franklin.[15] However, for energetic photons as considered here, the effect of this term might not necessarily be small, especially for the convection current contribution. We are currently implementing our calculation to include this rescattering contribution.

[1]M. Gari and H. Hebach, Phys. Rep. **72**, 1 (1981).

[2]S. Homma *et al.*, Phys. Rev. C **36**, 1623 (1987).

[3]E. Grosse *et al.*, Europhys. Lett. **2**, 9 (1986).

[4]J. Stevenson *et al.*, Phys. Rev. Lett. **57**, 555 (1986).

[5]N. Alamanos *et al.*, Phys. Lett. B **173**, 392 (1986).

[6]K. Kwato Njock *et al.*, Phys. Lett. B **175**, 125 (1986).

[7]H. Nifenecker and J. Bondorf, Nucl. Phys. **A442**, 478 (1985).

[8]C. M. Ko, G. F. Bertsch, and J. Aichelin, Phys. Rev. C **31**, 2324 (1985).

[9]W. Bauer *et al.*, Nucl. Phys. **A456**, 159 (1986).

[10]W. Cassing *et al.*, Phys. Lett. B **181**, 217 (1986).

[11]W. Bauer *et al.*, Phys. Rev. C **34**, 2127 (1986).

[12]K. Nakayama and G. F. Bertsch, Phys. Rev. C **34**, 2190 (1986).

[13]D. Neuhauser and S. E. Koonin, Nucl. Phys. **A462**, 163 (1987).

[14]B. A. Remington, M. Blann, and G. F. Bertsch, Phys. Rev. Lett. **57**, 2909 (1986); Phys. Rev. C **35**, 1720 (1987).

[15]V. R. Brown and J. Franklin, Phys. Rev. C **8**, 1706 (1973).

[16]V. R. Brown, Phys. Lett. **32B**, 259 (1970).

[17]L. S. Celenza *et al.*, Phys. Lett. **41B**, 283 (1972).

[18]G. E. Bohannon, L. Heller, and R. H. Thompson, Phys. Rev. C **16**, 284 (1977).

[19]M. K. Liou and K. S. Cho, Nucl. Phys. **A124**, 85 (1969); M. K. Liou and M. I. Sobel, Phys. Rev. C **4**, 1507 (1971).

[20]M. L. Goldberger and K. M. Watson, *Collision Theory* (Wiley, New York, 1964).

[21]R. Machleidt, K. Holinde, and Ch. Elster, Phys. Rep. **149**, 1 (1987).

[22]K. Nakayama and W. G. Love, Phys. Rev. C **38**, 51 (1988).

[23]F. P. Brady and J. C. Young, Phys. Rev. C **2**, 1579 (1970); **7**, 1707 (1973).

[24]K. Nakayama, S. Krewald, and J. Speth, Nucl. Phys. **A451**, 243 (1986).

[25]R. L. Workman and H. W. Fearing, Phys. Rev. C **34**, 780 (1986).

[26]H. W. Fearing, Nucl. Phys. **A463**, 95c (1987).

[27]J. P. Jeukenne, A. Lejeune, and C. Mahaux, Phys. Rep. **25C**, 83 (1976).

[28]J. Edgington and B. Rose, Nucl. Phys. **89**, 523 (1966).